X-ray Photoelectron Spectroscopy as a tool to investigate silane-based coatings for the protection of outdoor bronze: The role of alloying elements

This is a post-peer-review, pre-copyedit version of an article published in Progress in Organic Coatings. The final authenticated version of the paper "G. Masi, A. Balbo, J. Esvan, C. Monticelli, J. Avila, L. Robbiola, E. Bernardi, M.C. Bignozzi, M.C. Asensio, C. Martini, C. Chiavari, X-ray Photoelectron Spectroscopy as a tool to investigate silane-based coatings for the protection of outdoor bronze: The role of alloying elements, Applied Surface Science 433 (2018) 468–479" is available online at: https://doi.org/10.1016/j.apsusc.2017.10.089

X-ray Photoelectron Spectroscopy as a tool to investigate silane-based coatings for the protection of outdoor bronze: the role of alloying elements

G. Masi[1] A. Balbo[2], J. Esvan[3], C. Monticelli[2], J. Avila[4], L. Robbiola[5], E. Bernardi[6], M.C. Bignozzi[1], M.C. Asensio[4], C. Martini[7], C. Chiavari[8*]

[1] Dipartimento di Ingegneria Civile, Chimica, Ambientale e dei Materiali, Università di Bologna, via Terracini 28, 40131 Bologna (Italy) *giulia.masi5@unibo.it, maria.bignozzi@unibo.it*
[2] Centro di Studi sulla Corrosione e Metallurgia "A. Daccò", University of Ferrara, Via G. Saragat, 4/a, 44122 Ferrara (Italy) *andrea.balbo@unife.it, cecilia.monticelli@unife.it*
[3] Centre Interuniversitaire de Recherche et d'Ingénierie des Matériaux, Université de Toulouse, 4 allée Emile Monso, 31030 Toulouse (France) *jerome.esvan@ensiacet.fr*
[4] Synchrotron SOLEIL, L'Orme des Merisiers, 91190 Saint-Aubin (France) *jose.avila@synchrotron-soleil.fr, maria-carmen.asensio@synchrotron-soleil.fr*
[5] TRACES lab (CNRS UMR5608), Université de Toulouse, allées Antonio-Machado, 31058 Toulouse (France) *robbiola@univ-tlse2.fr*
[6] Dipartimento di Chimica Industriale "Toso Montanari", Università di Bologna, viale Risorgimento 4, 40136 Bologna (Italy) *elena.bernardi@unibo.it*
[7] Dipartimento di Ingegneria Industriale, Università di Bologna, viale Risorgimento 4, 40136 Bologna (Italy) *carla.martini@unibo.it*
[8] Dipartimento di Beni Culturali, Università di Bologna, via degli Ariani 1, 48121 Ravenna (Italy) *cristina.chiavari@unibo.it*

Abstract

Application of a protective coating is the most widely used conservation treatment for outdoor bronzes (cast Cu-Sn-Zn-Pb-Sb alloys). However, improving coating protectiveness requires detailed knowledge of the coating/substrate chemical bonding. This is particularly the case for 3-mercapto-propyl-trimethoxy-silane (PropS-SH) applied on bronze, exhibiting a good protective behaviour in outdoor simulated conditions.
The present work deals with X-Ray Photoelectron Spectroscopy (XPS) and Electron Microscopy (FEG-SEM+FIB (Focused Ion Beam)) characterization of a thin PropS-SH film on bronze. In particular, in order to better understand the influence of alloying elements on coating performance, PropS-SH was studied first on pure Cu and Sn substrates then on bronzes with increasing alloy additions: Cu8Sn as well as a quinary Cu-Sn-Zn-Pb-Sb bronze. Moreover, considering the real application of this coating on historical bronze substrates, previously artificially aged ("patinated") bronze samples were prepared and a comparison between bare and "patinated" quinary bronzes was performed. In the case of coated quinary bronze, the free

* Corresponding author: Tel. *0544-936780*

e-mail address: cristina.chiavari@unibo.it (Dr. Cristina Chiavari)

surface of samples was analysed by High Resolution Photoelectron Spectroscopy using Synchrotron Radiation (HR-SRPES) at ANTARES (Synchrotron SOLEIL), which offers a higher energy and lateral resolution. By compiling complementary spectroscopic and imaging information, a deeper insight into the interactions between the protective coating and the bronze substrate was achieved.

Keywords: X-ray Photoelectron Spectroscopy; bronze; silane coating; atmospheric corrosion; conservation-restoration; cultural heritage.

1. Introduction

Cultural Heritage in outdoor conditions naturally undergoes a degradation process that can severely damage the historical and cultural traces of this heritage. This is typically the case for outdoor bronzes, which suffer corrosion inducing specific patinas on metallic surfaces [1,2]. Particularly in urban atmosphere, corrosion phenomena lead to a marked degradation of bronze monuments, making patinas partially leachable, as demonstrated by green streaks on stone basements. In this context, the application of protective coatings remains the best solution for limiting corrosion damage of outdoor bronzes, as suggested in the last decades [3].

As regards protective treatments, organosilane coatings attracted a significant research attention in recent years, due to their protective efficiency towards the corrosion of several alloys in outdoor conditions. Research studies on the protection of copper and copper-based alloys were mainly carried out on octadecyl-trimethoxy-silane [4], glycidoxy-propyl-trimethoxy-silane [5] and γ-aminopropyltriethoxysilane (γ-APS) [6]. However, outstanding results were obtained with silanes containing sulphur or mercapto- groups, such as 3-mercapto-propyl-trimethoxy-silane (PropS-SH) [6–14].

The protective properties of PropS-SH coatings are connected to the formation of silanol groups (Si-OH) during silane hydrolysis and to their subsequent condensation in a polymeric dense Si-O-Si network [8].

On copper and copper alloys, surface chemisorption of PropS-SH through metal thiolate (Me-S-C) [7] and metal siloxane (Me-O-Si) bonds [15] ensures the desirable adhesion to the metal substrate.

In general, in the Cultural Heritage field the selection of protective coatings and corrosion inhibitors therein requires taking into account the following key points: (i) a basic understanding of the corrosion mechanism and (ii) testing the efficiency and the aesthetical impact of the candidate treatments on representative substrates, which reproduce in a reliable way the complexity of real surfaces. Therefore, in the present work, a quinary bronze was prepared with the typical microstructure and morphology of cast bronzes. Subsequently, investigation was performed with the aim to reproduce the typical corrosion features of unsheltered areas in real outdoor bronze monuments and to investigate the chemical bonding between coating and aged substrate (key point (ii)). Bronze samples were exposed to conditions closely simulating outdoor exposures [16,17] and in particular to runoff conditions (through dropping test). The tested protective coating was obtained from PropS-SH, selected on the basis of previous electrochemical tests and accelerated ageing tests performed on the same bronze alloy [11,13].

In order to achieve a better comprehension of the chemical bonds between Cu-based alloys and PropS-SH, Cu-based substrates with different alloying elements and pure tin were selected for the

application and study of PropS-SH coating. Specifically, beside tin, investigations were performed on pure copper, binary tin-bronze alloy (Cu8Sn) and the more complex quinary alloy, also aged under conditions similar to those induced by outdoor dropping rains. XPS spectroscopy is one of the most appropriate techniques to characterize coatings and their interaction with substrates. In particular, in this study concerning the coated bare quinary bronze, High Resolution Photoelectron Spectroscopy using Synchrotron Radiation (HR-SRPES) at ANTARES (Synchrotron SOLEIL) has been applied for the first time offering higher energies and lateral resolution [18].

2. Materials and methods

2.1 Materials

Quinary bronze was used as the main substrate for coating application. The composition of quinary bronze is: 91.9 Cu, 2.4 Sn, 1.0 Pb, 2.9 Zn and 0.8 Sb (wt%). It has a typical dendritic as-cast microstructure with cored α-solid solution (i.e. local enrichment of Sn and Sb elements in the interdendritic spaces) also including non-miscible lead globules as detailed in [12,14]. Shrinkage due to cooling during the casting process was also observed, inducing the formation of micro-cavities. Pure copper (Cu) and tin (Sn) metals (purity higher than 99.99 wt%), as well as a binary bronze alloy with 8 wt% Sn (Cu8Sn) were used as reference materials. Moreover, in order to investigate coating properties in the absence of interactions with bronze elements, also a non-metallic, ceramic substrate (zirconium nitride, ZrN) was prepared.

Only in the case of quinary bronze, both bare and patinated conditions were considered. The patination simulating natural patinas was performed by accelerated ageing test using a Dropping test device, described in detail elsewhere [17]. A synthetic rain solution (pH=4.3) was periodically dropped onto 45° inclined specimens through four rain channels per specimen, in order to maximize the aged surface, with alternated cycles of 2-days dropping/1-day drying, 3-days dropping/1-day drying. The Total Time of Wetness (ToW) was 30 days. The acid rain solution was prepared on the basis of ambient samples collected at a monitoring station in Bologna, Italy, with composition reported in [19]. The dropping tests simulate the runoff condition of outdoor bronzes due to unsheltered exposure to rainwater. The application of this accelerated ageing test was previously found to produce representative patinated substrates, comparable to natural patinas, suitable for testing protective treatments [20].

Artificially patinated quinary bronze was characterised by a rough surface, with a corrosion-modified layer of variable thickness, higher within the core of the dendrites than in the peripheral areas, due to preferential dissolution of copper and zinc from the alloy [12,14,17].

2.2 Preparation and characterisation of PropS-SH coating

Before coating application, the surfaces of bare samples were prepared by emery papers, then

polished by using diamond spray with decreasing particle size (down to 1 µm), washed with deionized water and degreased with acetone. Instead, the rough artificially patinated surface (quinary bronze) was silane coated without any surface preparation.

In order to prepare thin coatings suitable for XPS analysis of coating/metal interfaces, bare samples of Cu, Sn, Cu8Sn and quinary bronze were immersed ("dip-coated") for short times (150 s) in hydrolysed silane solution (90/5/5 v/v ethanol/water/PropS-SH) at pH= 4, followed by fast withdrawal (Table 1). Then, the samples were washed by ethanol to eliminate physisorbed silane molecules. The obtained coatings were few nanometers thick as evaluated by weight gain measurements, assuming a density value of 1.1 $g.cm^{-3}$ for PropS-SH. By prolonging to 1 hour the immersion time in hydrolysed silane solution, thicker coatings on ZrN were prepared, which permitted to investigate the coating bulk on a corrosion resistant substrate by XPS (Table 1).

1 h dip coating is often adopted for PropS-SH to protect efficiently bronzes from corrosion [11–14]. Therefore on patinated quinary bronze, these thicker coatings were also applied to analyse their cross section stratigraphy and for surface XPS and HR-SRPES investigations.

All the coated samples were cured at room temperature for at least 10 days before analyses. Finally, uncoated bare quinary bronze were used as representative substrate for XPS measurements in order to check the initial state of bronze surface before coating application. The surface was analysed after the polishing previously described.

XPS analysis, performed on the samples collected in Table 1, was carried out by using a monochromatised Al Kα (hν = 1486.7 eV) source on a ThermoScientific K-Alpha system. The X-ray spot size was about 400 µm. The pass energy was fixed at 130 eV with a step of 1 eV for surveys and 40 eV with a step of 0.1 eV for core levels. Ionic Ar^+ sputtering of the surfaces was not applied in order to avoid modifications of the organosilane. The analysed core levels (C 1s, O 1s, Si 2p, S 2p, Cu 2p, Zn 2p, Sn 3d, Pb 4f) were calibrated against C 1s binding energy (conventionally BE=284.6±0.1 eV). XPS data were fitted by using Thermo Scientific™ Avantage Software and the background signal was removed by using Shirley method. Flood gun was also applied for avoiding charge effects.

Table 1: *Samples on which XPS measurements were carried out: summary of sample acronyms and coating application conditions.*

Bare and patinated quinary bronze samples carrying thick PropS-SH coatings were investigated by Scanning Electron Microscopy (SEM) coupled with Energy Dispersive Spectroscopy (EDS) (Zeiss EP EVO 50 in variable pressure mode (80 Pa) with an EDS X-ray detector Oxford Instruments INCA Energy 350 [z > 4 (Be)]) as well as by High Resolution Photoelectron Spectroscopy using Synchrotron Radiation (HR-SRPES) with excitation energy of 700 eV, as already detailed in a previous work [18]. Imaging of the free coated surface was carried out using the R4000 Scienta hemispherical analyser with a set of Fresnel Zone Plates (FZP), able to focalise the beam spot up to a

few tenths of nanometres in spatial resolution [21,22]. The main difference of the ANTARES microscope from other conventional ARPES instruments is that the specimens can be mounted on a high-precision plate that ensures their nanoscale positioning in the x, y and z directions [18,21,22]. HR-SRPES experiments were conducted in the ANTARES beam line at the SOLEIL synchrotron. HR-SRPES chemical imaging maps were recorded on the same surface areas where EDS maps were subsequently collected.

From these samples, cross-sections were prepared by Focused Ion Beam (FIB) milling and the coating/substrate morphology was investigated by combining a Ga^+ ion beam and a thermal field emission SEM, working at coincidence on the sample (FEI Dual Beam Strata 235M System) [18]. For FIB cross-sections, a protective Pt-C layer was deposited on top of the surface before milling, so as to protect the surface features.

3. Results and discussion

3.1 Thick PropS-SH coatings on quinary bronze

Starting from the most representative system of real outdoor bronzes, images of thick PropS-SH coatings on quinary bronze obtained by 1h immersion are shown in Figure 1 for both bare (left-hand side) and artificially patinated (right-hand side) samples. In Figures 1a and b, the low magnification tilted images of the free surface reveal different features when PropS-SH coating is applied on bare or patinated bronze, highlighting the influence of the substrate. In particular, they show that PropS-SH adapts tightly to the surface morphology of the substrate, so that a very smooth and planar surface is achieved on the polished alloy, while the initial rough morphology is still observed on the patinated sample.

SEM images of the micrometric cross-section slices prepared by FIB lift-out technique are reported in Figures 1c-f for the same samples. Figures 1c and d give a general view of bare and patinated bronze cross-sections respectively, while higher magnification images are reported in Figures 1e and f, so allowing a better identification of microstructural details and layer sequence. In both cases, the Pt-C overlayer (for protection during FIB milling) is visible above the organosilane coating.

The application of PropS-SH on bare bronze (Figures 1a, c and e) produces a rather homogeneous layer with an average thickness of about 0.3 μm. However, when PropS-SH is applied by 1h immersion on the uneven patinated bronze (Figures 1b, d and f), the coating fills up the localised corrosion areas forming a layer with variable thickness (dark grey in Figures 1d and f). Figure 1d shows a crater of corrosion preferentially developed within the brighter grain on the right-hand side corresponding to dendrite core, being the grain microstructure of the bronze highlighted thanks to the electron channelling contrast.

Figure 1: *SEM observation of PropS-SH coatings on quinary bronze substrate. Left-hand side (a, c, e): bare bronze / Right-hand side (b, d, f): patinated bronze. (a, b) PropS-SH coating surfaces; (c, d, e, f) cross-sections prepared by FIB (Focused Ion Beam) lift-out technique.*

In order to investigate more deeply the elemental distribution within the PropS-SH coating on quinary bronze, EDS and HR-SRPES maps of elemental distribution were collected in the same locations on the free surface of the coated bare bronze samples.

EDS maps are reported in Figure 2 for a typical area where the PropS-SH coating covers a shrinkage micro-cavity at the dendrite border, located in the centre of each image. Regarding the characteristic elements belonging to PropS-SH, C and O show a relatively homogeneous distribution, while Si and S exhibit locally higher intensities in correspondence with the shrinkage micro-cavity. Hence, the more intense signal of Si and of S is related to a possible accumulation of PropS-SH, filling up this cavity. In addition, due to the low thickness of the silane coating (~300 nm), also X-rays emission from bronze alloying elements is detected, revealing the microstructure of the as-cast bronze with Sn micro-segregation in the interdendritic space.

Figure 2: *PropS-SH on bare quinary bronze, SEM/EDS analysis of the free surface: SE image and X-ray maps of the main elements (C, O, Si, S, Cu, Sn and Pb).*

HR-SRPES chemical imaging brings complementary information about coating elements distribution: it is worth noting that in the case of HR-SRPES only the top surface (a few nm) of the coating is investigated, while EDS results reveal the alloying element distribution underneath the coating as previously discussed.

Figure 3a reports the optical observation of the same area where EDS maps of Figure 2 were collected and where HR-SRPES maps of Figures 3b-d were recorded as well. It shows some colorimetric interference surrounding the central micro-porosity in the middle of the image. This could be linked to small variations of coating thickness according to a different elemental distribution on the surface, as revealed in Figures 3b-d, related to the HR-SRPES maps of C 1s, O 1s and Si 2p at a micrometric scale.

In fact, these signals are rather strong in the area surrounding the cavity, while they are absent in the cavity itself. Conversely, EDS Si and O signals are more intense into the cavity than outside it and decrease towards the dendrite core, as shown by the Sn distribution map in Figure 2, highlighting microstructural features. These observations suggest that the organosilane coating accumulates at the bottom of the cavity (as shown by EDS signals, coming from a higher depth than HR-SRPES), replicating the surface topography, while it is not detectable in the upper volume of the cavity itself (as suggested by HR-SRPES signal from the uppermost layer) because the coating does not level up completely the surface. This is probably due to the relatively low viscosity of the adopted silane solution and to capillary effects, which allow its penetration into recessed features.

Figure 3: *PropS-SH on bare quinary bronze, free surface: optical image (a) and HR-SRPES maps for C 1s, O1s and Si 2p (b-d). The optical image (a) shows the analysed area, corresponding to the same location of Figure 2: the yellow dashed square indicates the area covered by HR-SRPES maps (side of the square=100 μm) (b-d).*

3.2 XPS analysis: PropS-SH-coated metals and alloys and uncoated quinary bronze

In order to deeply investigate the coating-substrate bonding system, which is very important for understanding PropS-SH protective properties both on bare and patinated bronze, XPS analyses on coated samples and on uncoated bare quinary bronze were performed, using a larger spot size than in HR-SRPES and taking into account very thin PropS-SH deposits on Cu, Sn, Cu8Sn and bare quinary bronze, so as to investigate the coating-substrate interface. Tests on ZrN and patinated quinary bronze, both coated by 1h immersion, and uncoated quinary bronze were also performed to investigate, respectively, the coating bulk, a sample more representative of a real coated system and the bronze substrate before coating application. Elemental Zn was not taken into consideration as a reference material, because in patinated bronze Zn is selectively dissolved in the environment, so that it is no more detected in patinas [23,24]. To help comprehension of the following results, Table 2 reports the values of XPS peak positions of the main elements detected on the top surfaces of the different PropS-SH coated samples in this study.

Table 2: *Binding energies of the different chemical species detected in XPS core levels.*

Figure 4: *XPS surveys of PropS-SH layer on: (a) ZrN, (b) Cu, (c) Sn, (d) Cu8Sn, (e) bare quinary bronze, (f) patinated quinary bronze and (g) uncoated bare quinary bronze (BQ), (thin coatings in (b), (c), (d) and (e)).*

Figure 5: *XPS core levels of the characteristic PropS-SH elements on the different substrates (thin coatings on Cu, Sn, Cu8Sn, and Q): (a) C 1s, (b) O 1s, (c) Si 2p and (d) S 2p.*

Figure 6: *XPS core level of Sn 3d measured on (a) pure Sn coated with PropS-SH; (b) quinary (thin coating); (c) quinary patinated bronze and (d) uncoated bare quinary bronze (BQ).*

ZrN (reference substrate)

The obtained XPS surveys are reported in Figure 4. Figure 4a refers to PropS-SH layer on ZrN and it shows intense peaks of the characteristic elements of the coating (C 1s, O 1s, Si 2p, S 2s and S 2p). No signal from the substrate (Zr 3d and N 1s) is detected, suggesting that, as expected, the spectrum in Figure 4a is not affected by the substrate/coating interface and can be considered as a reference one for PropS-SH coating.

The core level spectra of C 1s, O 1s, Si 2p and S 2p are reported in Figure 5a-d, respectively. C1s spectrum in Figure 5a shows a sharp peak centred at 284.5 eV (BE), typical of aliphatic chain (C-H bond) of PropS-SH and atmospheric compounds adsorbed on the surface. Characteristic contributions of silane layer are highlighted by O 1s and Si 2p levels at binding energies of 531.9 eV (O1s core level spectra of Figure 5b) and 101.8 eV (S2p core level spectra of Figure 5c). These BE values indicate a main contribution of the Si-O-Si bonds, suggesting a good grade of reticulation of the coating [9,25,26]. Figure 5d evidences that the contribution of S $2p_{3/2}$ is centred at 162.9 eV, representative of S-C bonds [27]. In particular, the analysis of S 2p signal takes into account the presence of a doublet structure of the core level with a spacing of 1.2 eV (S $2p_{1/2}$ - S $2p_{3/2}$ = 1.2 eV) and a theoretical intensity ratio of 2 (S $2p_{3/2}$/S $2p_{1/2}$=2). No evidence of unreacted thiol groups (-SH) usually occurring at around 163.5 eV (BE) [9,28] was observed in the S 2p core level, likely due to prevalent adsorption through metal-thiolate bonds [29].

Pure Cu

XPS survey of the thin PropS-SH layer applied on pure Cu substrate is reported in Figure 4b. Characteristic elements of the coating (C 1s, O 1s, Si 2p, S 2s and S 2p) are clearly detected as previously observed for the coating reference, as well as the intense signal of the substrate (Cu 2p). In particular, Figure 5 shows the main contributions of C 1s, O 1s, Si 2p and S 2p, centred at binding energies of 284.5 eV, 531.9 eV, 101.7 eV and 162.6 eV, respectively. C 1s signal also shows some small contributions at higher binding energies (Figure 5a), that is at 286.2 eV and 288.3 eV, corresponding to C-S / C-O and O=C-O, respectively. The former C 1s contribution (C-S) is typical of the studied silane molecule, while the latter suggests that some PropS-SH oxidation occurs [13]. On this substrate, S 2p signal shows two different contributions: S $2p_{3/2}$ BE=162.6 eV, ascribed to S-Cu thiolate bond [9,10,30] or S-C, and BE=168.2 eV, mainly related to sulfate, as better distinguishable in Figure 5d. It is well known that the partial oxidation of the thiol groups can occur in the presence of oxygen gas contamination [31,32] and it is catalysed by the presence of multiple-valence cations (like Cu and Sn ions), among which copper ions show high catalytic effects [31]. This justifies the presence of oxidized species on coated Cu, but not on coated ZrN, as from zirconium element only zirconium (IV) cations can be formed. It is significant that the thiol group oxidation occurs concurrently to the oxidation of silane aliphatic chain.

Pure Sn

XPS survey of coated pure Sn (Figure 4c) shows weaker peak intensities of the characteristic elements of PropS-SH, in comparison to pure Cu. In particular, contributions at higher BE for C 1s (BE = 286.2 and 288.3 eV) are more intense than those on Cu, indicating a higher degree of oxidation (Figure 5a). Figure 5 b shows that for O 1s a shoulder at BE=530.4 eV occurs, typical of oxide species linked to Sn. Si 2p and S 2p signals (Figure 5c and d) are with scarce intensity, noisy and characterized by

broad peaks. For S 2p signal (Figure 5d), the contributions due to the S-Sn/S-C environment (BE=162.5 eV) and to SO_x (BE=168.5 eV) are comparable.

Figure 6a shows the characteristics of Sn 3d core level detected on coated Sn metal. Sn 3d exhibits three different contributions at 484.7 eV, 485.9 eV and 486.7 eV, corresponding to metallic Sn, Sn(II) oxide (SnO) and/or Sn(II)-S, and Sn(IV) oxide (SnO_2) with a possible Sn-SO_x contribution, in good accordance with literature data [33–37]. Here the distinction between Sn(II) and Sn(IV) peaks has been performed assuming a FWHM value of 1.3 eV and 1.5 eV, respectively. These findings indicate the formation of a thinner PropS-SH coating on pure Sn compared to pure Cu substrate and suggest that the Sn oxidized species can have a considerable catalytic effect in the oxidation of thiol group inducing the formation of significant amounts of poorly soluble SO_x compounds.

Cu8Sn and quinary bronze (Cu2Sn3Zn1Pb1Sb)

When a PropS-SH film is applied by fast dip coating on bare bronze samples, the XPS survey spectra of Figures 4 d-e are recorded, showing similar features to those observed in Cu and Sn spectra (Figure 4 b-c). In particular, intense peaks belonging to PropS-SH are observed, but among the alloying elements of the substrates only Cu signal is clearly visible.

In Cu8Sn (Figure 4d), the Sn $3d_{5/2}$ level shows a very low and poorly resolved signal, with a main contribution at BE=486.4 eV, attributed to Sn(IV) oxide and only a small peak at BE=484.8 eV linked to metallic Sn, as reported in the literature [33]. In quinary bronze (Figure 4e), all alloying elements except copper (Sn 3d, Zn 2p, Sb 3d, Pb 4f) exhibit undetectable or low intensity XPS peaks. In particular, Figures 6b show the Sn 3d core levels on this substrate which indicate the presence of both metallic and oxidised Sn(IV) species, at 484.7 eV and 486.7 eV respectively [17]. Pb $4f_{7/2}$ level centred at BE = 138.6 eV and Zn $2p_{3/2}$ level centred at BE = 1022.1 eV (core levels not shown) are linked to oxygen-containing species [18,38]. As some of these elements are in significant concentration in bronzes (e.g. tin in Cu8Sn), in general their absence or negligible detection by XPS indicates that PropS-SH produces relatively abundant continuous coatings on bronze substrates.

Regarding the characteristic PropS-SH elements, Figure 5 evidences that the chemical environments for C 1s, O 1s, Si 2p and S 2p detected on both bare bronzes are corresponding to those on pure Cu substrate. This suggests that the minor alloying elements do not affect the coating-bronze bonds: the coating correctly adheres onto the substrates, with a similar binding mechanism, which is essentially due to the formation of metal-thiolate bonds, involving Cu and Sn atoms, the latter being at a relatively minor extent.

Also on coated bronzes, the oxidation of the thiol group in the coating occurs in conjunction with oxidation of the silane aliphatic chain, as already observed for pure Cu and Sn. The peculiar influence of copper and bronze alloying elements on this degradation process is likely responsible of its occurrence on these substrates.

Quinary bronze vs. patinated quinary bronze

Figure 4f shows the XPS survey of thick coated patinated bronze surface. In contrast to the thin bare quinary bronze (Figure 4e), the characteristic elements of the coating (C 1s, O 1s, Si 2p and S 2p) are more clearly detected, while the characteristic peaks of the substrate, like Cu 2p, Zn 2p, Sn 3d and Pb 4f, are less intense. As far as Sn 3d core levels in the presence of these substrates (Figures 6b and c), it is clear that, while both metallic and oxidised Sn(IV) species are detected on bare quinary bronze at 484.7 eV and 486.7 eV, respectively, on patinated bronze reasonably only Sn(IV) species related to Sn-rich corrosion products are observed [17].

On coated patinated quinary bronze, some environmental elements linked to the corrosion process in acid rain solution are also recorded on the XPS survey, such as N 1s and Ca 2p centred at 400 eV and 347 eV, respectively (Figure 4f). The increase of -SO_x contributions for S 2p is also linked to the formation of sulfates among the corrosion products. All the characteristic elements of the coating show peaks similar in position and concentration to those obtained on coated quinary bare bronze. However, O 1s peak is broader and shows, in addition, a contribution at higher BE (~ 534 eV), indicating a remarkable presence of oxide and/or hydroxide compounds linked to copper and related to corrosion products on the top surface (Figure 5b).

Uncoated bare quinary bronze (BQ)

XPS survey of the uncoated bare quinary bronze (BQ) is reported in Figure 4g. As expected, the spectrum shows the characteristics contributions of the alloying elements (Pb 4f, Sn 3d and Cu 2p), except for Zn that was not detected. In particular, Figure 6d shows the Sn core level spectrum recorded on uncoated quinary bronze just after polishing and before coating application, highlighting the presence of a predominant peak at 485.7 eV connected to Sn(II) oxide and a minor peak compatible with Sn(0). Dip coating in aerated silane hydroalcoholic solution is likely responsible of further oxidation of the pre-existing Sn(II) oxide film into the oxidised Sn(IV) species, detected under the PropS-SH coating, as shown by Figure 6a.

Figure 7: *(a) Cu 2p core levels and (b) Cu-LMM Auger spectra measured on Cu, Cu8Sn and quinary (thin coatings), on quinary patinated bronze and on uncoated bare quinary bronze (BQ) (from the top to the bottom, respectively).*

Auger

Cu 2p core level and Auger spectra (Cu LMM) are reported in Figures 7a and 7b respectively, for coated pure Cu, bare bronzes (Cu8Sn and quinary bronze), patinated quinary bronze substrate and uncoated bare quinary bronze. A very similar chemical environment for Cu core levels is found for the coated samples. In particular, Cu 2p core levels show the typical features of the oxidation state of copper (I) with just a very small shake-up satellite peak, more developed for quinary bronze after accelerated ageing by Dropping test. The Cu $2p_{3/2}$ peak is centred at 933.1 eV (BE), while the Auger

Cu $L_3M_{4,5}M_{4,5}$ signal at 915.6 eV (KE), with modified Auger parameter (α'), is measured at around 1848.7 eV. These values well correspond to Cu(I) species, such as a mix of cuprous oxide and Cu(I)-S bonds [39]. For patinated quinary bronze coated by PropS-SH, copper contribution is low and the Cu 2p core level, as well as the Auger signal, is noisy and not well resolved. Conversely, the uncoated bare quinary bronze shows a Cu environment slightly different. In particular, Cu 2p core level shows the features of a mix of Cu(0) and Cu(I) species, with the Cu $2p_{3/2}$ peak centred at 932.5 eV (BE). The Auger Cu $L_3M_{4,5}M_{4,5}$ signal at 918.0 eV (KE), with modified Auger parameter (α') measured at around 1850.5 eV, are characteristic of Cu(0) species, as reported in [40,41]. This confirms the fact that coating application is likely responsible of further oxidation of the pre-existing Cu(0) in Cu(I) species.

XPS atomic quantification on the top surface of PropS-SH coated substrates

From the analysis of the XPS core levels, it is possible to evaluate the atomic concentration of the different elements on the coated surfaces. These values, together with their concentrations normalized with respect Si relative amount, are reported in Table 3.

On all samples, high C concentrations are detected but, due to surface C contamination, no meaningful trend among the samples is evident. O level always shows comparable atomic concentrations in all samples, except for PropS-SH applied on pure Sn, in which O concentration is higher (1.5 times higher than in the reference sample), due to abundant formation of tin oxides and sulphates. In general, the coated ZrN substrate shows the lowest O atomic concentration, because the coating is rather thick and the coating/material interface (where oxide accumulation may occur) cannot be investigated. On this reference substrate, the concentrations of the coating elements (C 1s, O 1s, S 2p) normalized to silicon are in very good agreement with the theoretical atomic ratios (O/Si=1.5, C/Si=3.0 and S/Si=1.0). This suggests that the coating reticulation is almost complete and no significant silane oxidation occurs.

On coated metallic substrates, Si concentrations decrease by passing from pure Cu to either bare or patinated bronze, to pure Sn, indicating a decreasing coating build-up, as the tin content of the substrate increases. Also total S atomic concentration decreases by passing from Cu and Cu-based alloys to Sn, but without a monotonic trend. Oxidation of the thiol group up to sulphate ion occurs at various extents on all bare metals and the low total S/Si ratios detected on Cu and bronze substrates, in comparison to the expected value of 1 (based on silane stoichiometry), suggest partial sulphate dissolution during dip coating. Only on Sn substrate, the ratio (total S)/Si ratio is close to 1 (0.6+0.5), due to significant amount of insoluble sulphate species detected, likely linked to the formation of insoluble compounds with Sn(IV), as suggested by Sn core level spectrum. The concentration of S involved in S-Metal and C-S bonds, normalized to that of silicon, is particularly low in the case of Cu

substrate, indicating that thiol oxidation in PropS-SH is more evident on pure copper than on bronze or pure Sn.

Regarding the characteristic elements of the metallic substrates, Cu 2p signal is about double on coated bare bronze substrates in comparison to pure Cu, so confirming the lower average PropS-SH thickness on the former substrate types than on pure Cu. On patinated quinary bronze, where decuprification occurs due to selective corrosion, the lowest copper concentration is detected. On this substrate, the relatively high sum of the alloying element content (> 1.3 at%) is a consequence of the decrease in Cu at%, but may be also connected to the non-uniform distribution of PropS-SH, which does not avoid the emergence of the rough surface patina.

Table 3: *XPS atomic quantification on the top surface of PropS-SH coated substrates (at%). Each concentration value has been normalised to Si atomic content (/Si at%).*

4. Conclusions

The following conclusions could be drawn from these results:

- XPS technique allowed the collection of detailed information about the interaction of the organosilane coating (PropS-SH) with bronze including the role of the main alloying elements in artistic alloys (Sn, Zn and Pb).

- PropS-SH coatings tightly follow the morphology of the substrate on which they are applied. In particular, EDS and HR-SRPES maps on bare quinary bronze evidence that these coatings sink into shrinkage cavities, filling them up and forming a homogenous and continuous thin layer (< 500 nm). On patinated quinary bronze, the coating penetrates into the porosities apparently insulating the bronze substrate.

- 1h dip coating applied to the ZrN substrate produces rather thick coatings, which allow the characterisation of the coating itself by XPS. Atomic quantification data related to the coating and normalized to Si signal are in good accordance with theoretical values, indicating that coating reticulation is almost complete and no silane oxidation occurs.

- More uniform and likely thicker silane layers form by passing from pure Sn to bronze to pure Cu. In all cases, the contribution of Cu- and (where present) Sn-thiolate bonds to silane adhesion has been recognized.

- An appreciable tendency of PropS-SH coating to oxidation is detected, with formation of sulfate and carboxylate groups. The extent of this phenomenon depends on the substrate

nature: it is more evident on pure copper than on bronze or pure Sn. It does not occur on ZrN. It likely takes place during the dip coating step and appears to be favoured by the presence of multiple-valence cations.

Acknowledgements

All the personnel from the SOLEIL synchrotron facility (Proposal n. 20150149) and the IPANEMA laboratory (Gif Sur Yvette, France) is gratefully acknowledged for their very effective technical support. This work has been performed in the scope of the B-IMPACT project within M-ERA.NET network, supported by national funding organisations ((MIZŠ, MIUR, RMP). The authors wish also to thank Dr. Gian Carlo Gazzadi at CNR NANO, Modena for FIB-FEG/SEM analyses.

References

[1] L. Robbiola, H.P. Hurtel, Nouvelle contribution à l'étude des mécanismes de corrosion des bronzes de plein air: caractérisation de l'altération de bronzes de Rodin, (1991) 809–823.

[2] A. Krätschmer, I. Odnevall Wallinder, C. Leygraf, The evolution of outdoor copper patina, Corros. Sci. 44 (2002) 425–450. doi:10.1016/S0010-938X(01)00081-6.

[3] M. Marabelli, G. Napolitano, Nuovi sistemi protettivi applicabili su opere o manufatti in bronzo esposti all'aperto, Mater. E Strutt. 1 (1991) 51–56.

[4] F. Zucchi, V. Grassi, A. Frignani, G. Trabanelli, C. Monticelli, Octadecyl-trimethoxy-silane film formed on copper in different conditions, Mater. Chem. Phys. 103 (2007) 340–344. doi:10.1016/j.matchemphys.2007.02.050.

[5] F. Deflorian, S. Rossi, L. Fedrizzi, M. Fedel, Integrated electrochemical approach for the investigation of silane pre-treatments for painting copper, Prog. Org. Coatings. 63 (2008) 338–344. doi:10.1016/j.porgcoat.2008.03.005.

[6] C. Rahal, M. Masmoudi, M. Abdelmouleh, R. Abdelhedi, An environmentally friendly film formed on copper: Characterization and corrosion protection, Prog. Org. Coatings. 78 (2015) 90–95. doi:10.1016/j.porgcoat.2014.09.018.

[7] R.J. Tremont, D.R. Blasini, C.R. Cabrera, Controlled self-assembly of mercapto and silane terminated molecules at Cu surfaces, J. Electroanal. Chem. 556 (2003) 147–158. doi:10.1016/S0022-0728(03)00340-1.

[8] F. Zucchi, A. Frignani, V. Grassi, G. Trabanelli, M. Dal Colle, The formation of a protective layer of 3-mercapto-propyl-trimethoxy-silane on copper, Corros. Sci. 49 (2007) 1570–1583. doi:10.1016/j.corsci.2006.08.019.

[9] F. Sinapi, S. Julien, D. Auguste, L. Hevesi, J. Delhalle, Z. Mekhalif, Monolayers and mixed-layers on copper towards corrosion protection, Electrochim. Acta. 53 (2008) 4228–4238. doi:10.1016/j.electacta.2007.12.061.

[10] Y.S. Li, W. Lu, Y. Wang, T. Tran, Studies of (3-mercaptopropyl)trimethoxylsilane and bis(trimethoxysilyl)ethane sol-gel coating on copper and aluminum, Spectrochim. Acta - Part A Mol. Biomol. Spectrosc. 73 (2009) 922–928. doi:10.1016/j.saa.2009.04.016.

[11] A. Balbo, A. Frignani, C. Monticelli, Influence of nanoparticles on the inhibiting efficiency of organosilane coatings on bronze. Part 1: Electrochemical characterization, in: Eurocorr 2012 (EFC Event n.330), EFC, London, UK, 2012: p. 1–8 (Paper: 1524).

[12] A. Balbo, C. Chiavari, C. Martini, C. Monticelli, Effectiveness of corrosion inhibitor films for the conservation of bronzes and gilded bronzes, Corros. Sci. 59 (2012) 204–212. doi:10.1016/j.corsci.2012.03.003.

[13] C. Chiavari, A. Balbo, E. Bernardi, C. Martini, F. Zanotto, I. Vassura, et al., Organosilane coatings applied on bronze: Influence of UV radiation and thermal cycles on the

protectiveness, Prog. Org. Coatings. 82 (2015) 91–100. doi:10.1016/j.porgcoat.2015.01.017.

[14] C. Chiavari, A. Balbo, E. Bernardi, C. Martini, M.C. Bignozzi, M. Abbottoni, et al., Protective silane treatment for patinated bronze exposed to simulated natural environments, Mater. Chem. Phys. 141 (2013) 502–511. doi:10.1016/j.matchemphys.2013.05.050.

[15] W.J. van Ooij, D. Zhu, M. Stacy, A. Seth, T. Mugada, J. Gandhi, et al., Corrosion Protection Properties of Organofunctional Silanes—An Overview, Tsinghua Sci. Technol. 10 (2005) 639–664. doi:10.1016/S1007-0214(05)70134-6.

[16] C. Chiavari, E. Bernardi, C. Martini, F. Passarini, F. Ospitali, L. Robbiola, The atmospheric corrosion of quaternary bronzes: The action of stagnant rain water, Corros. Sci. 52 (2010) 3002–3010. doi:10.1016/j.corsci.2010.05.013.

[17] E. Bernardi, C. Chiavari, B. Lenza, C. Martini, L. Morselli, F. Ospitali, et al., The atmospheric corrosion of quaternary bronzes: The leaching action of acid rain, Corros. Sci. 51 (2009) 159–170. doi:10.1016/j.corsci.2008.10.008.

[18] G. Masi, C. Chiavari, J. Avila, J. Esvan, S. Raffo, M.C. Bignozzi, et al., Corrosion investigation of fire-gilded bronze involving high surface resolution spectroscopic imaging, Appl. Surf. Sci. 366 (2016) 317–327. doi:10.1016/j.apsusc.2016.01.101.

[19] C. Chiavari, E. Bernardi, A. Balbo, C. Monticelli, S. Raffo, M.C. Bignozzi, et al., Atmospheric corrosion of fire-gilded bronze: corrosion and corrosion protection during accelerated ageing tests, Corros. Sci. 100 (2015) 435–447. doi:http://dx.doi.org/10.1016/j.corsci.2015.080.013.

[20] C. Chiavari, E. Bernardi, C. Martini, L. Morselli, F. Ospitali, L. Robbiola, et al., Predicting the corrosion behaviour of outdoor bronzes: assessment of artificially exposed and real outdoor samples, Met. 2010 Proc. Interim Meet. ICOM-CC Met. Work. Group, Oct. 11-15, 2010, Charleston, South Carolina, USA. (2011) 218–226.

[21] J. Avila, I. Razado-Colambo, S. Lorcy, J. Giorgetta, F. Polack, M.C. Asensio, Interferometer-controlled soft X-ray scanning photoemission microscope at SOLEIL, J. Phys. Conf. Ser. 425 (2013) 132013. doi:10.1088/1742-6596/425/13/132013.

[22] J. Avila, I. Razado-Colambo, S. Lorcy, B. Lagarde, J. Giorgetta, F. Polack, et al., ANTARES, a scanning photoemission microscopy beamline at SOLEIL, J. Phys. Conf. Ser. 425 (2013) 192023. doi:10.1088/1742-6596/425/19/192023.

[23] E. Bernardi, C. Chiavari, C. Martini, L. Morselli, The atmospheric corrosion of quaternary bronzes: An evaluation of the dissolution rate of the alloying elements, Appl. Phys. A Mater. Sci. Process. 92 (2008) 83–89. doi:10.1007/s00339-008-4451-0.

[24] C. Chiavari, K. Rahmouni, H. Takenouti, S. Joiret, P. Vermaut, L. Robbiola, Composition and electrochemical properties of natural patinas of outdoor bronze monuments, Electrochim. Acta. 52 (2007) 7760–7769. doi:10.1016/j.electacta.2006.12.053.

[25] F. Sinapi, J. Delhalle, Z. Mekhalif, XPS and electrochemical evaluation of two-dimensional organic films obtained by chemical modification of self-assembled monolayers of (3-

mercaptopropyl) trimethoxysilane on copper surfaces, Mater. Sci. 22 (2002) 345–353. doi:10.1016/S0928-4931(02)00210-2.

[26] P.M. Dietrich, S. Glamsch, C. Ehlert, A. Lippitz, N. Kulak, W.E.S. Unger, Synchrotron-radiation XPS analysis of ultra-thin silane films : Specifying the organic silicon, Appl. Surf. Sci. 363 (2016) 406–411.

[27] M. Finšgar, 2-Mercaptobenzimidazole as a copper corrosion inhibitor: Part II. Surface analysis using X-ray photoelectron spectroscopy, Corros. Sci. 72 (2013) 90–98. doi:10.1016/j.corsci.2013.03.010.

[28] Z. Mekhalif, L. Massi, F. Guittard, S. Geribaldi, J. Delhalle, X-Ray photoelectron spectroscopy study of polycrystalline zinc modified by n -dodecanethiol and 3-perfluorooctyl-propanethiol, 405 (2002) 186–193.

[29] M. Kozelj, A.S. Vuk, I. Jerman, B. Orel, Corrosion protection of Sunselect, a spectrally selective solar absorber coating, by (3-mercaptopropyl)trimethoxysilane, Sol. Energy Mater. Sol. Cells. 93 (2009) 1733–1742. doi:10.1016/j.solmat.2009.05.023.

[30] F. Sinapi, I. Lejeune, J. Delhalle, Z. Mekhalif, Comparative protective abilities of organothiols SAM coatings applied to copper dissolution in aqueous environments, Electrochim. Acta. 52 (2007) 5182–5190. doi:10.1016/j.electacta.2006.12.087.

[31] G.A. Bagiyan, I.K. Koroleva, N. V Soroka, A. V Ufimtsev, Oxidation of thiol compounds by molecular oxygen in aqueous solutions, Russ. Chem. Bull. 52 (2003) 1135–1141. doi:10.1023/A:1024761324710.

[32] W. Sui, W. Zhao, X. Zhang, S. Peng, Z. Zeng, Q. Xue, Comparative anti-corrosion properties of alkylthiols SAMs and mercapto functional silica sol-gel coatings on copper surface in sodium chloride solution, J. Sol-Gel Sci. Technol. 80 (2016) 567–578. doi:10.1007/s10971-016-4108-y.

[33] L. Kövér, Z. Kovács, R. Sanjinés, G. Moretti, I. Cserny, G. Margaritondo, et al., Electronic structure of tin oxides: High‐resolution study of XPS and Auger spectra, Surf. Interfa. 23 (1995) 461–466. http://onlinelibrary.wiley.com/doi/10.1002/sia.740230705/full (accessed May 30, 2016).

[34] L. Robbiola, T.T.M. Tran, P. Dubot, O. Majerus, K. Rahmouni, Characterisation of anodic layers on Cu-10Sn bronze (RDE) in aerated NaCl solution, Corros. Sci. 50 (2008) 2205–2215. doi:10.1016/j.corsci.2008.06.003.

[35] P. Sinsermsukakul, L. Sun, S. Lee, H. Park, S. Kim, C. Yang, et al., Overcoming efficiency limitations of SnS-based solar cells, Adv. Energy Mater. (2014) 1400496. http://faculty.chemistry.harvard.edu/files/gordon/files/prasertadvenergymater2014.pdf (accessed June 1, 2016).

[36] J.A. Rodriguez, T. Jirsak, S. Chaturvedi, J. Hrbek, Surface chemistry of SO2 on Sn and

Sn/Pt(111) alloys: Effects of metal- metal bonding on reactivity toward sulfur, J. Am. Chem. Soc. 120 (1998) 11149–11157. doi:10.1021/ja982174a.

[37] M. Hutchison, P. Zhou, K. Ogle, J. Scully, Enhanced Electrochemical Cu Release from Commercial Cu-Sn Alloys: Fate of the Alloying Elements in Artificial Perspiration, Electrochim. Acta. (2017). doi:10.1016/j.electacta.2017.04.092.

[38] A. Galtayries, A. Mongiatti, P. Marcus, C. Chiavari, Surface characterisation of corrosion inhibitors on bronzes for artistic casting, Corros. Met. Herit. Artefacts Investig. Conserv. Predict. Long Term Behav. 48 (2007) 335–351. doi:10.1533/9781845693015.335.

[39] F. Zucchi, A. Frignani, V. Grassi, G. Trabanelli, M. DalColle, The formation of a protective layer of 3-mercapto-propyl-trimethoxy-silane on copper, Corros. Sci. 49 (2007) 1570–1583. doi:10.1016/j.corsci.2006.08.019.

[40] C. Debiemme-Chouvy, F. Ammeloot, E.M.M. Sutter, X-ray photoemission investigation of the corrosion film formed on a polished Cu-13Sn alloy in aerated NaCl solution, Appl. Surf. Sci. 174 (2001) 55–61.

[41] S. Colin, E. Beche, R. Berjoan, H. Jolibois, A. Chambaudet, An XPS and AES study of the free corrosion of Cu-, Ni- and Zn-based alloys in synthetic sweat, Corros. Sci. 41 (1999) 1051–1065. doi:10.1016/S0010-938X(98)00141-3.

Figure captions

Figure 1: *SEM observation of PropS-SH coatings on quinary bronze substrate. Left-hand side (a, c, e): bare bronze / Right-hand side (b, d, f): patinated bronze. (a, b) PropS-SH coating surfaces; (c, d, e, f) cross-sections prepared by FIB (Focused Ion Beam) lift-out technique.*

Figure 2: *PropS-SH on bare quinary bronze, SEM/EDS analysis of the free surface: SE image and X-ray maps of the main elements (C, O, Si, S, Cu, Sn and Pb).*

Figure 3: *PropS-SH on bare quinary bronze, free surface: optical image (a) and HR-SRPES maps for C 1s, O1s and Si 2p (b-d). The optical image (a) shows the analysed area, corresponding to the same location of Figure 2: the yellow dashed square indicates the area covered by HR-SRPES maps (side of the square=100 μm) (b-d).*

Figure 4: *XPS surveys of PropS-SH layer on: (a) ZrN, (b) Cu, (c) Sn, (d) Cu8Sn, (e) bare quinary bronze, (f) patinated quinary bronze and (g) uncoated bare quinary bronze (BQ), (thin coatings in (b), (c), (d) and (e)).*

Figure 5: *XPS core levels of the characteristic PropS-SH elements on the different substrates (thin coatings on Cu, Sn, Cu8Sn, and Q): (a) C 1s, (b) O 1s, (c) Si 2p and (d) S 2p.*

Figure 6: *XPS core level of Sn 3d measured on (a) pure Sn coated with PropS-SH; (b) quinary (thin coating); (c) quinary patinated bronze and (d) uncoated bare quinary bronze (BQ).*

Figure 7: *(a) Cu 2p core levels and (b) Cu-LMM Auger spectra measured on Cu, Cu8Sn and quinary (thin coatings), on quinary patinated bronze and on uncoated bare quinary bronze (BQ) (from the top to the bottom, respectively).*

Figures

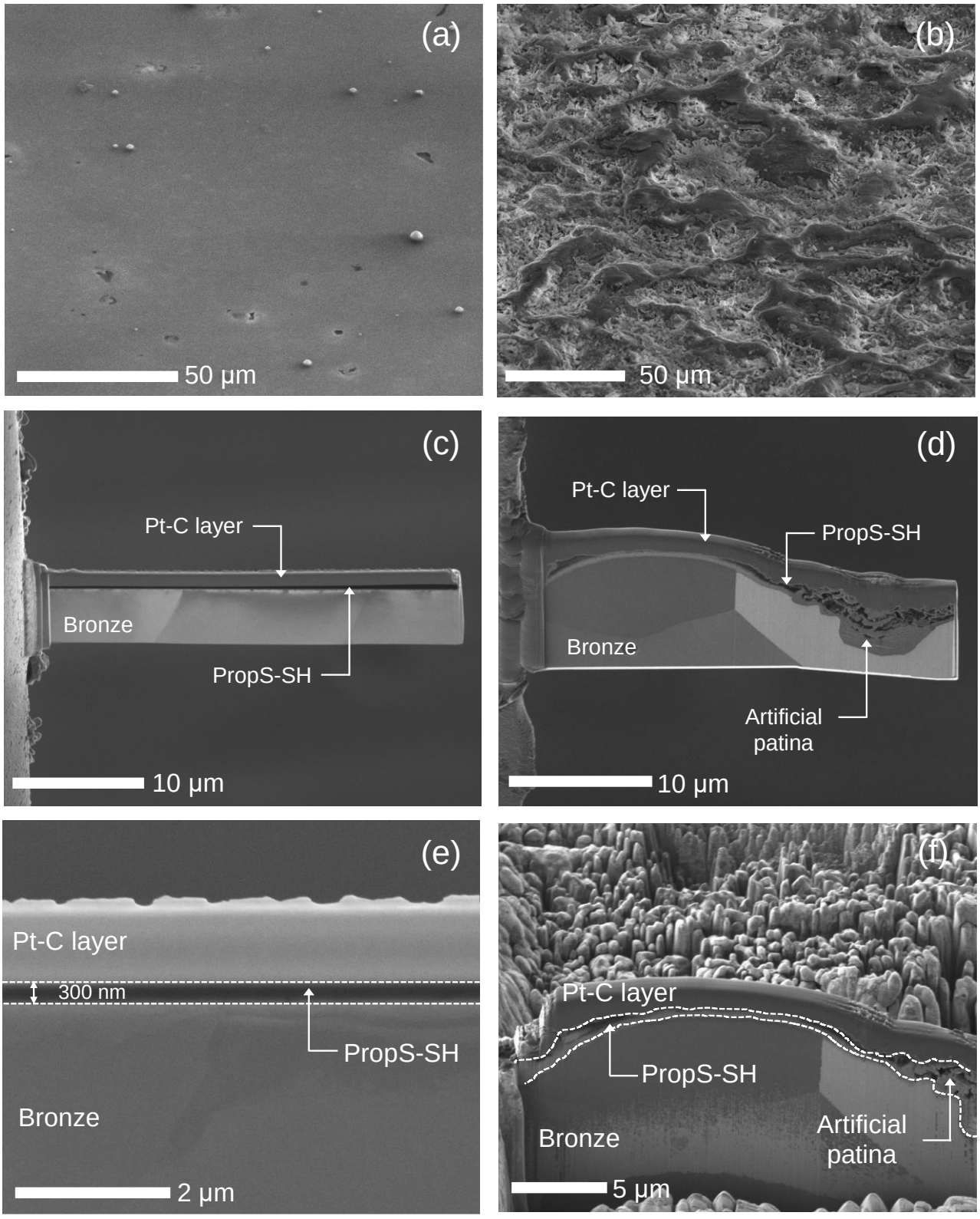

Figure 1

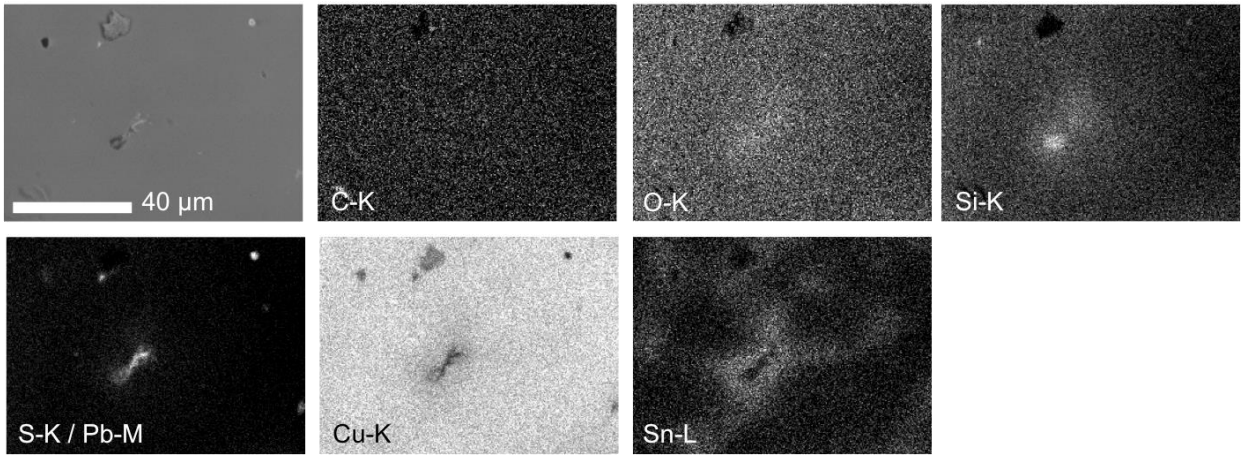

Figure 2

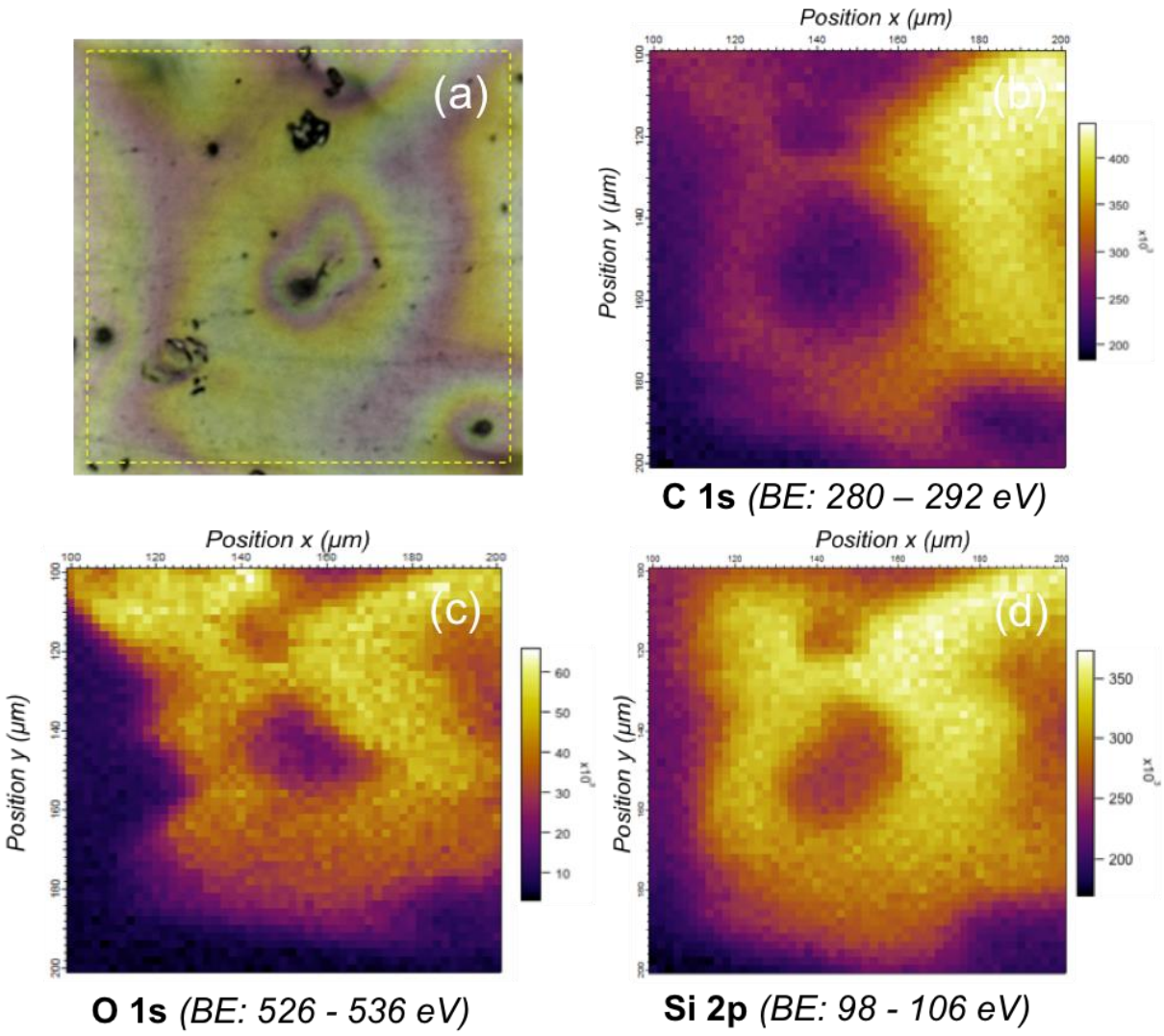
(a)
Position x (µm)
Position y (µm)
(b)
C 1s (BE: 280 – 292 eV)
(c)
O 1s (BE: 526 - 536 eV)
(d)
Si 2p (BE: 98 - 106 eV)

Figure 3

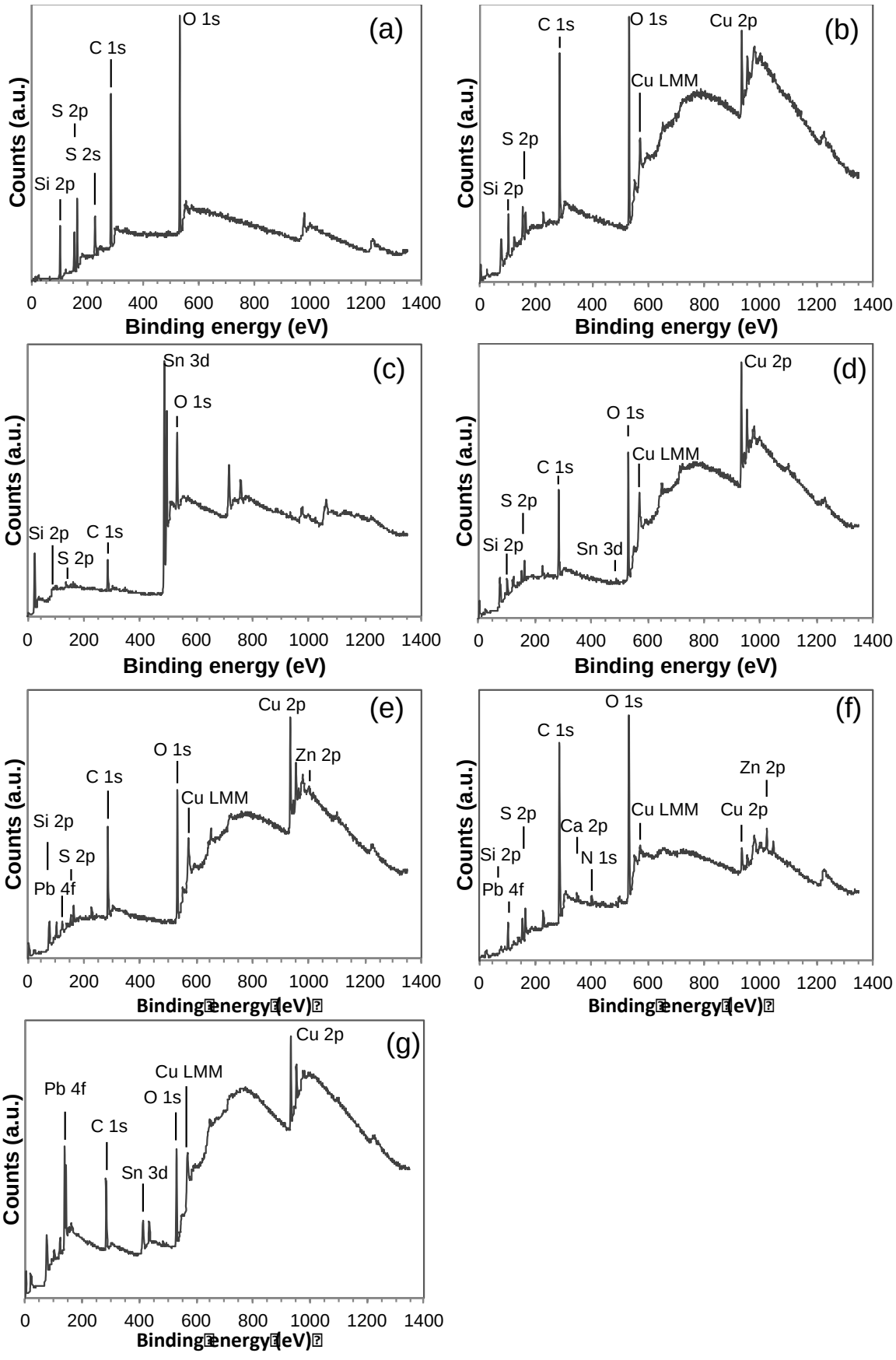
(a)
O 1s
C 1s
S 2p
S 2s
Si 2p
Counts (a.u.)
0 200 400 600 800 1000 1200 1400
Binding energy (eV)
(b)
C 1s
O 1s
Cu 2p
Cu LMM
S 2p
Si 2p
Counts (a.u.)
0 200 400 600 800 1000 1200 1400
Binding energy (eV)
(c)
Sn 3d
O 1s
Si 2p
C 1s
S 2p
Counts (a.u.)
0 200 400 600 800 1000 1200 1400
Binding energy (eV)
(d)
Cu 2p
O 1s
Cu LMM
C 1s
S 2p
Si 2p
Sn 3d
Counts (a.u.)
0 200 400 600 800 1000 1200 1400
Binding energy (eV)
(e)
Cu 2p
O 1s
Zn 2p
C 1s
Cu LMM
Si 2p
S 2p
Pb 4f
Counts (a.u.)
0 200 400 600 800 1000 1200 1400
Binding energy (eV)
(f)
O 1s
C 1s
Zn 2p
S 2p
Ca 2p
Cu LMM
Cu 2p
Si 2p
N 1s
Pb 4f
Counts (a.u.)
0 200 400 600 800 1000 1200 1400
Binding energy (eV)
(g)
Cu 2p
Cu LMM
Pb 4f
O 1s
C 1s
Sn 3d
Counts (a.u.)
0 200 400 600 800 1000 1200 1400
Binding energy (eV)

Figure 4

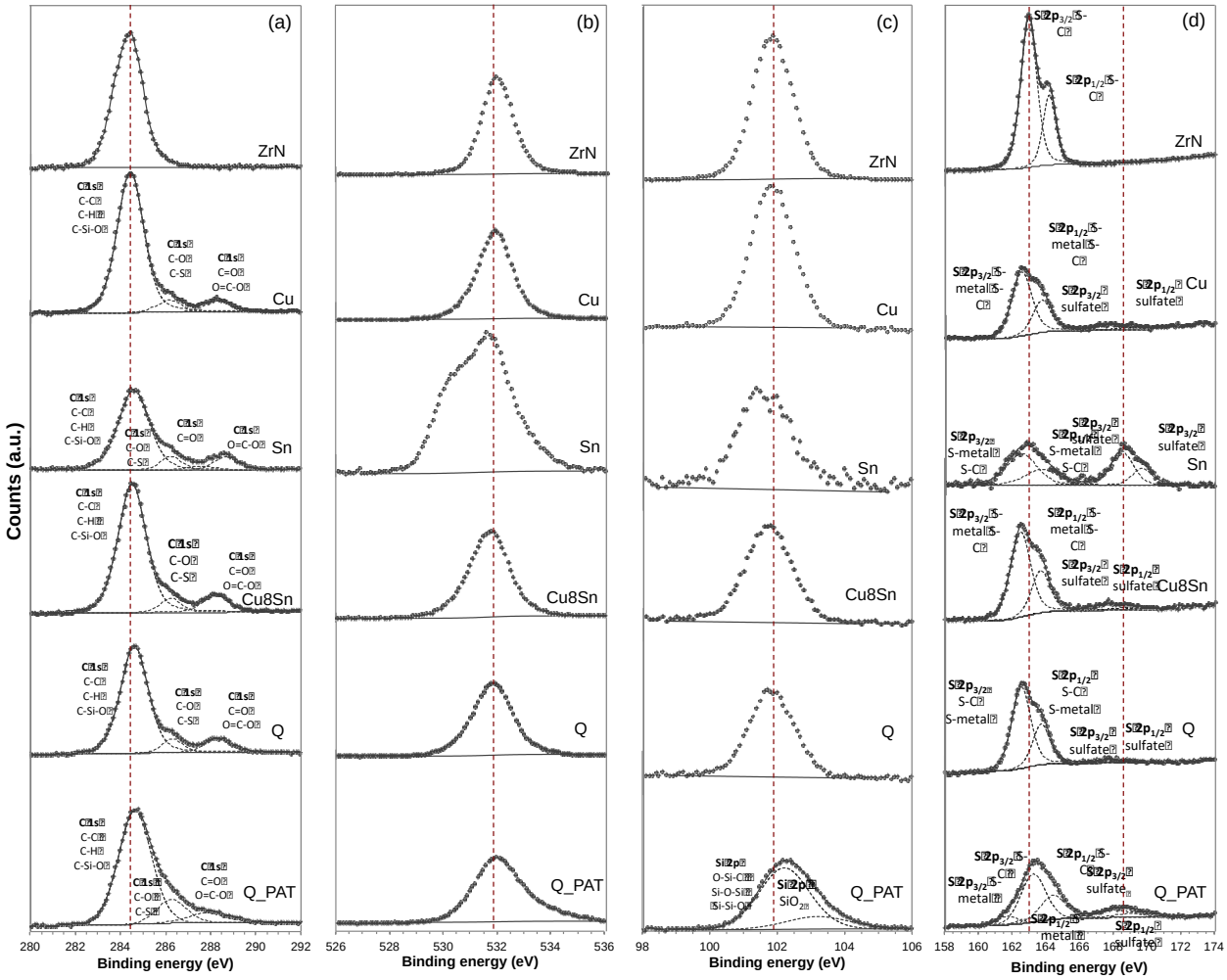
(a)
(b)
(c)
(d)
ZrN
Cu
Sn
Cu8Sn
Q
Q_PAT
Counts (a.u.)
Binding energy (eV)
C1s
C-C
C-H
C-Si-O
C-O
C-S
C=O
O=C-O
Si2p
O-Si-C
Si-O-Si
Si-Si-O
SiO2n
Si2p3/2-Cl
Si2p1/2-Cl
Si2p3/2-metal-Cl
Si2p1/2-metal-Cl
Si2p3/2 sulfate
Si2p1/2 sulfate
Si2p3/2n S-metal
Si2p3/2n S-C
Si2p1/2 S-Cl
Si2p1/2 S-metal
Si2p3/2-metal
Si2p1/2-metal

Figure 5

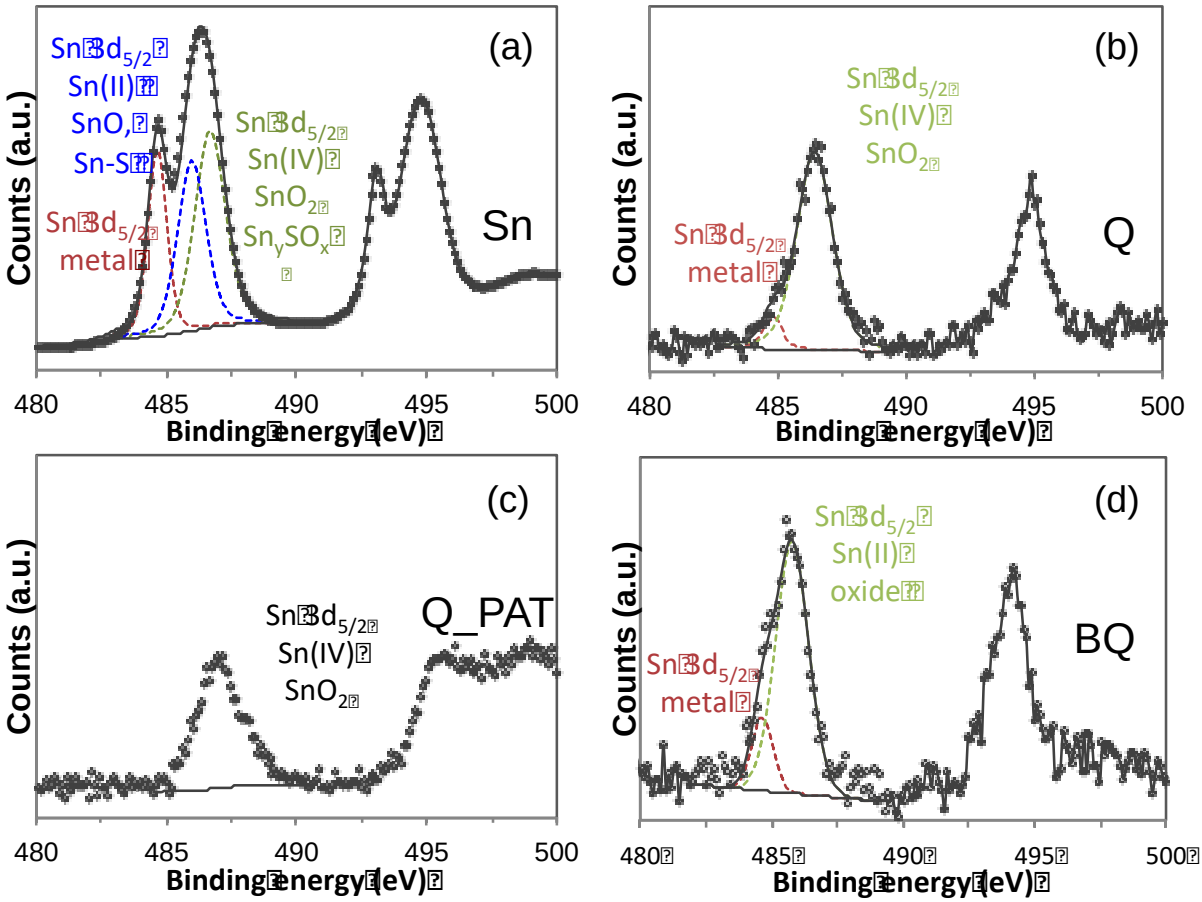
(a)
Sn 3d5/2
Sn(II)
SnO,
Sn-S
Sn 3d5/2
Sn(IV)
SnO2
SnySOx
Sn 3d5/2
metal
Sn
Counts (a.u.)
480
485
490
495
500
Binding energy (eV)
(b)
Sn 3d5/2
Sn(IV)
SnO2
Sn 3d5/2
metal
Q
Counts (a.u.)
480
485
490
495
500
Binding energy (eV)
(c)
Sn 3d5/2
Sn(IV)
SnO2
Q_PAT
Counts (a.u.)
480
485
490
495
500
Binding energy (eV)
(d)
Sn 3d5/2
Sn(II)
oxide
Sn 3d5/2
metal
BQ
Counts (a.u.)
480
485
490
495
500
Binding energy (eV)

Figure 6

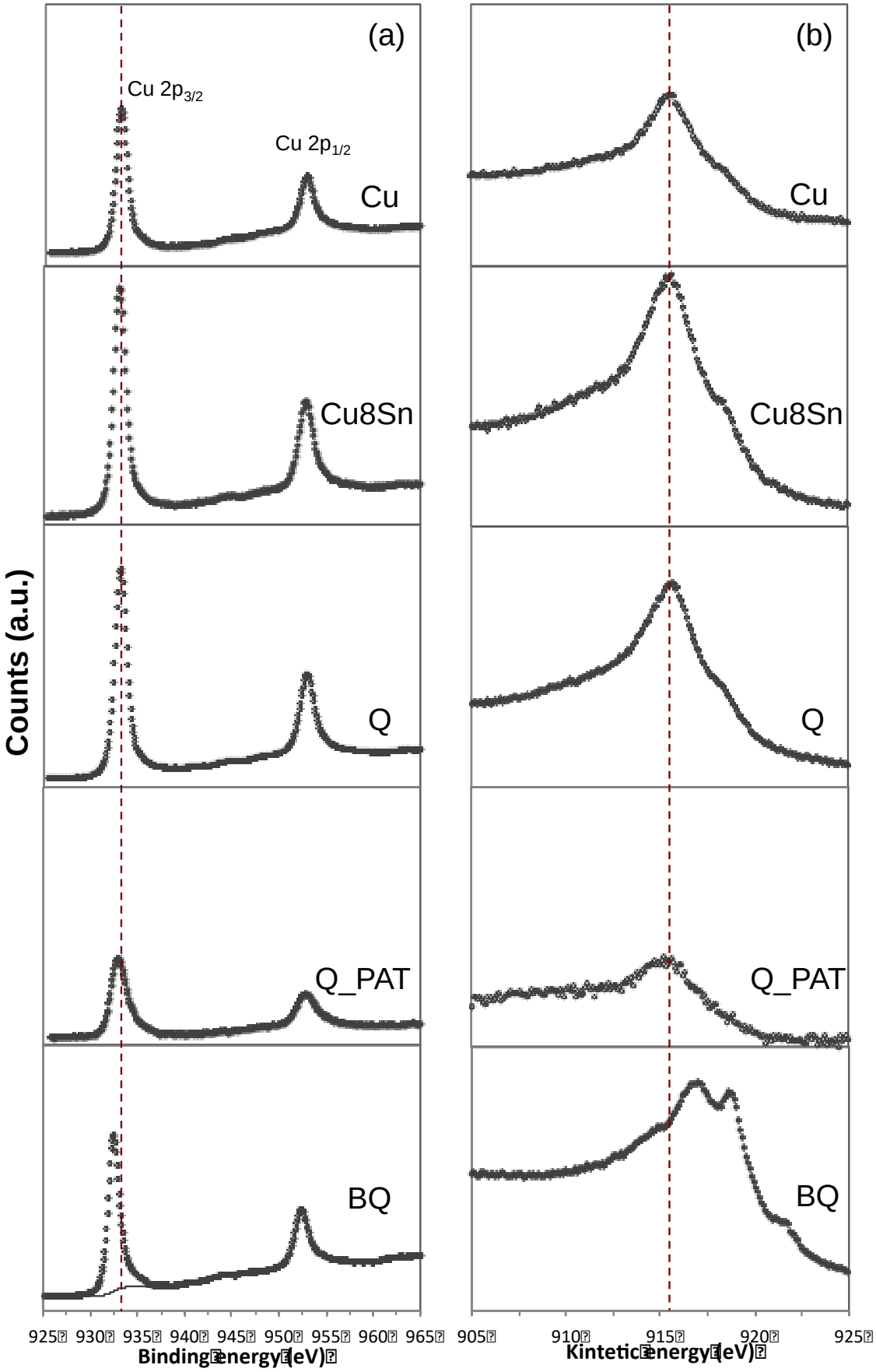
(a)
(b)
Cu 2p3/2
Cu 2p1/2
Cu
Cu8Sn
Q
Q_PAT
BQ
Counts (a.u.)
925 930 935 940 945 950 955 960 965
Binding energy (eV)
905 910 915 920 925
Kinetic energy (eV)

Figure 7

Tables

Table 1: *Samples on which XPS measurements were carried out: summary of sample acronyms and coating application conditions.*

Sample name	*Substrate*	*Coating*	*Application mode*
BQ	Bare Quinary Bronze	No Coating	-
ZrN	Zirconium nitride	PropS-SH (thick layer)	Dip-coating (1h immersion in silane sol.)
Cu	Pure copper	PropS-SH	Dip-coating (fast immersion in silane sol.)
Sn	Pure tin	PropS-SH	Dip-coating (fast immersion in silane sol.)
Cu8Sn	Binary bronze (8wt% Sn)	PropS-SH	Dip-coating (fast immersion in silane sol.)
Q	Quinary bronze	PropS-SH	Dip-coating (fast immersion in silane sol.)
Q_PAT	Patinated quinary bronze	PropS-SH	Dip-coating (1h immersion in silane sol.)

Table 2: *Binding energies of the different chemical species detected in XPS core levels.*

Element	*Peak*	*Position (eV)*	*References*
C 1s	CC, CH, C—Si C-O, C—S C=O, O=C-O	284.5 286.2 288.3	[9,10]
O 1s	-	531.8	[9,25]
Si 2p	C-Si-O, Si—O—Si Si-O (SiO_2)	101.7 103.2	[9,10,25,26]
S $2p_{3/2}$	S-C, S-Metal sulfates	162.5 168.5	[9,10,27,28,30]
Cu $2p_{3/2}$	Cu(0)	932.5*	[18,38,40,41]
	Cu (I)	933.1**	[8]
Zn $2p_{3/2}$	Oxide	1022.1	[18,38]
Sn $3d_{5/2}$	Metal Sn(II) Sn(IV)	484.7 485.9 486.7	[33–37]
Pb $4f_{7/2}$	Oxide	138.7	[18,38]

* KE (Cu LMM) = 918.0 eV; α' = 1850.5 eV – Cu(0) component

** KE (Cu LMM) = 915.6 eV; α' = 1848.7 eV – Cu(I) component

Table 3: *XPS atomic quantification on the top surface of PropS-SH coated substrates (at%). Each concentration value has been normalised to Si atomic content (/Si at%).*

	C			*O*	*Si*		*S*		*Cu*		*Zn*	*Sn*			*Pb*
	CC, C—H, C—Si	*C—O, C—S*	*C=O, O=C-O*		*C—Si—O, Si—O—Si*	*SiO_2*	*S—Metal, C-S*	*Sulfate*	*Cu(0)-Cu(I)*	*Cu(I)*	*Oxide*	*Metal*	*Sn(IV)*	*Sn(II)*	*Oxide*
BQ															
at%	42.2	5.2	7.4	30.9	-	-	-	-	9.4	-	-	0.1	-	0.3	4.8
ZrN															
at%	47.3	-	-	22.9	16.3	-	13.5	-	-	-	-	-	-	-	-
Normalised (/Si at%)	2.9	-	-	1.4	1.0	-	0.8	-	-	-	-	-	-	-	-
Cu															
at%	43.0	3.4	3.1	25.4	13.2	-	5.5	0.5	-	5.9	-	-	-	-	-
Normalised (/Si at%)	3.3	0.3	0.2	1.9	1.0	-	0.4	0.04	-	0.4	-	-	-	-	-
Sn															
at%	25.8	3.3	4.9	36.1	4.1	-	2.5	1.9	-	-	-	5.3	8.9	7.2	-
Normalised (/Si at%)	6.3	0.8	1.2	8.8	1.0	-	0.6	0.5	-	-	-	1.3	2.2	1.8	-
Cu8Sn															
at%	38.5	3.2	4.7	25.6	8.6	-	6.4	0.5	-	12.4	-	0.1	0.1	-	-
Normalised (/Si at%)	4.5	0.4	0.5	2.9	1.0	-	0.7	0.06	-	1.4	-	0.01	0.01	-	-
Q															
at%	38.9	3.8	4.8	25.7	8.0	-	6.7	0.3	-	11.8	0.1	-	0.1	-	0.3
Normalised (/Si at%)	4.9	0.5	0.6	3.2	1.0	-	0.8	0.04	-	1.5	0.01	-	0.01	-	0.04
Q_PAT															
at%	40.5/7.6/4.7	7.5	4.7	24.4	7.9	2.0	5.8	1.1	-	1.6	1.0	-	0.2	-	0.1
Normalised (/Si at%)	4.1	0.8	0.5	2.5	1.0		0.6	0.1	-	0.2	0.1	-	0.02	-	0.01